Australian Journal of Earth Sciences: An International Geoscience Journal of the Geological Society of Australia
Publication details, including instructions for authors and subscription information:
http://www.tandfonline.com/loi/taje20

East-west shortening during north-south convergence, example of the NW Himalayan syntaxis

A. Replumaz [a], V. Vignon [a], V. Regard [b], J. Martinod [b] & N. Guerrero [b]

[a] ISTerre, Université de Grenoble 1, CNRS, F-38041, Grenoble, France

[b] GET-Université de Toulouse-CNRS-IRD-OMP, 14 av. E. Belin, 31400, Toulouse, France

Version of record first published: 30 Jul 2012

To cite this article: A. Replumaz, V. Vignon, V. Regard, J. Martinod & N. Guerrero (2012): East-west shortening during north-south convergence, example of the NW Himalayan syntaxis, Australian Journal of Earth Sciences: An International Geoscience Journal of the Geological Society of Australia, 59:6, 845-858

To link to this article: http://dx.doi.org/10.1080/08120099.2012.701232

Australian Journal of Earth Sciences (2012) **59**, (845–858)

East–west shortening during north–south convergence, example of the NW Himalayan syntaxis

A. REPLUMAZ[1]*, V. VIGNON[1], V. REGARD[2], J. MARTINOD[2] AND N. GUERRERO[2]

[1]*ISTerre, Université de Grenoble 1, CNRS, F-38041 Grenoble, France.*
[2]*GET-Université de Toulouse-CNRS-IRD-OMP, 14 av. E. Belin, 31400 Toulouse, France.*

The northwest terminus of the Himalayan range forms a syntaxis limited by two strike-slip faults, the Chaman Fault to the west, and the Karakorum Fault to the east. In between these faults, smaller-scale syntaxes are observed, as the Nanga Parbat and the Kashmir syntaxes. The fold axial traces of these syntaxes trend nearly north–south, revealing a component of east–west shortening in the geodynamic context of the north–south convergence between India and Asia. We constructed a sandbox with two edges oblique to the convergence to test the influence of the NW Himalayan syntaxis large-scale structural geometry on the construction of a wedge and on its evolution. We used sand and microbeads as standard analogues for brittle crustal layers approximately 30 km thick. We show that the obliquity of the edges can generate an east–west shortening in a north–south convergence. The amount of east–west shortening generated by the oblique edges of the box is up to 40% of the amount of the north–south convergence. This shortening is accommodated by oblique motion on transpressive faults parallel to the edges. The amount of strike-slip motion is up to 60% of the convergence vector. We conclude that the obliquity of the edges is sufficient to generate an east–west shortening in a north–south convergence, but not sufficient to generate a north–south axial-trending fold. One experiment, with a free southern boundary, allowed the development of pure strike-slip faults within the sand layer, conjugated to pure shortening on one north–south fold. The east–west component of the oblique motion generated by the obliquity of the faults bordering the NW Himalayan syntaxis could be absorbed by a north–south fold as the Nanga Parbat if the motion on the border faults is pure strike-slip.

KEY WORDS: NW Himalayan syntaxis, double oblique convergent wedge, partitioning, indentation, convexity of Himalaya range, Pakistan.

INTRODUCTION

The Himalayan Arc is an accretionary wedge, which has been forming during the collision of India with Asia since the Eocene. The shape of the wedge is arcuate, convex toward the north (Figure 1a). At the NW terminus of the wedge, the arc forms a syntaxis with a shape convex toward the south. To the west, the Indian continent is limited by the Chaman Fault (Figure 1), a lithospheric strike-slip fault that accommodates the northwards sliding of India since the Eocene (e.g. Replumaz & Tapponnier 2003). To the east, the Karakorum strike-slip Fault connects to the subduction of Asian lithosphere beneath the Pamir fault (e.g. Negredo *et al.* 2007; Figure 1b) and partially accommodates the eastwards motion of Tibet (e.g. Avouac & Tapponnier 1993). The Chaman, the Karakorum and the Pamir Faults define a block of coherent deformation (Replumaz & Tapponnier 2003), with several thrusts approximately parallel to the Main Frontal Thrust (MFT, Figure 1). The northern Main Kohistan Thrusts (MKT) separates the thin and soft Asian crust from the Kohistan volcanic Arc. The Main Mantle Thrust (MMT) separates the Kohistan Arc from the thick and stiff Indian craton. Tomographic cross-sections show that India subducts northwards beneath the Hindu Kush and the Himalayas, and Asia subducts southwards beneath the Pamir region (Negredo *et al.* 2007). Beneath the Himalayas, seismic reflection profiles show that the Indian crust is sliced by thrusts parallel to the MFT (Main Boundary Thrust, MBT, Main Central Thrust, MCT), which merge at depth on an intracrustal decollement level (Main Himalayan Thrust, MHT; e.g.; Zhao *et al.* 1993). The MHT dips gently northward between 5.5 and 8° (Berger *et al.* 2004). The MHT occurs at the contact between the Lower Siwaliks group and the pre-Tertiary basement. Beneath the Salt Range, the MHT is shallower, lying within a thick Eo-Cambrian salt layer, and gently dips between 1 and 4° (Grelaud *et al.* 2002).

Several small-scale syntaxes have been described within the NW Himalayan syntaxis (e.g. Burbank 1983; Coward *et al.* 1987), including the Nanga Parbat syntaxis to the north and the Kashmir syntaxis to the south (Figure 1). The Nanga Parbat syntaxis

*Corresponding author: anne.replumaz@ujf-grenoble.fr

ISSN 0812-0099 print/ISSN 1440-0952 online
http://dx.doi.org/10.1080/08120099.2012.701232

corresponds to a crustal-scale N–S elongated dome. It folds the MMT into a broad N–S anticline in a regime of east–west shortening (Seeber & Pêcher 1998). Cooling ages indicate a rapid exhumation phase since 5 Ma, followed by an extension phase since 2 Ma (Schneider *et al.* 1999). Beneath the massif, the microseismicity

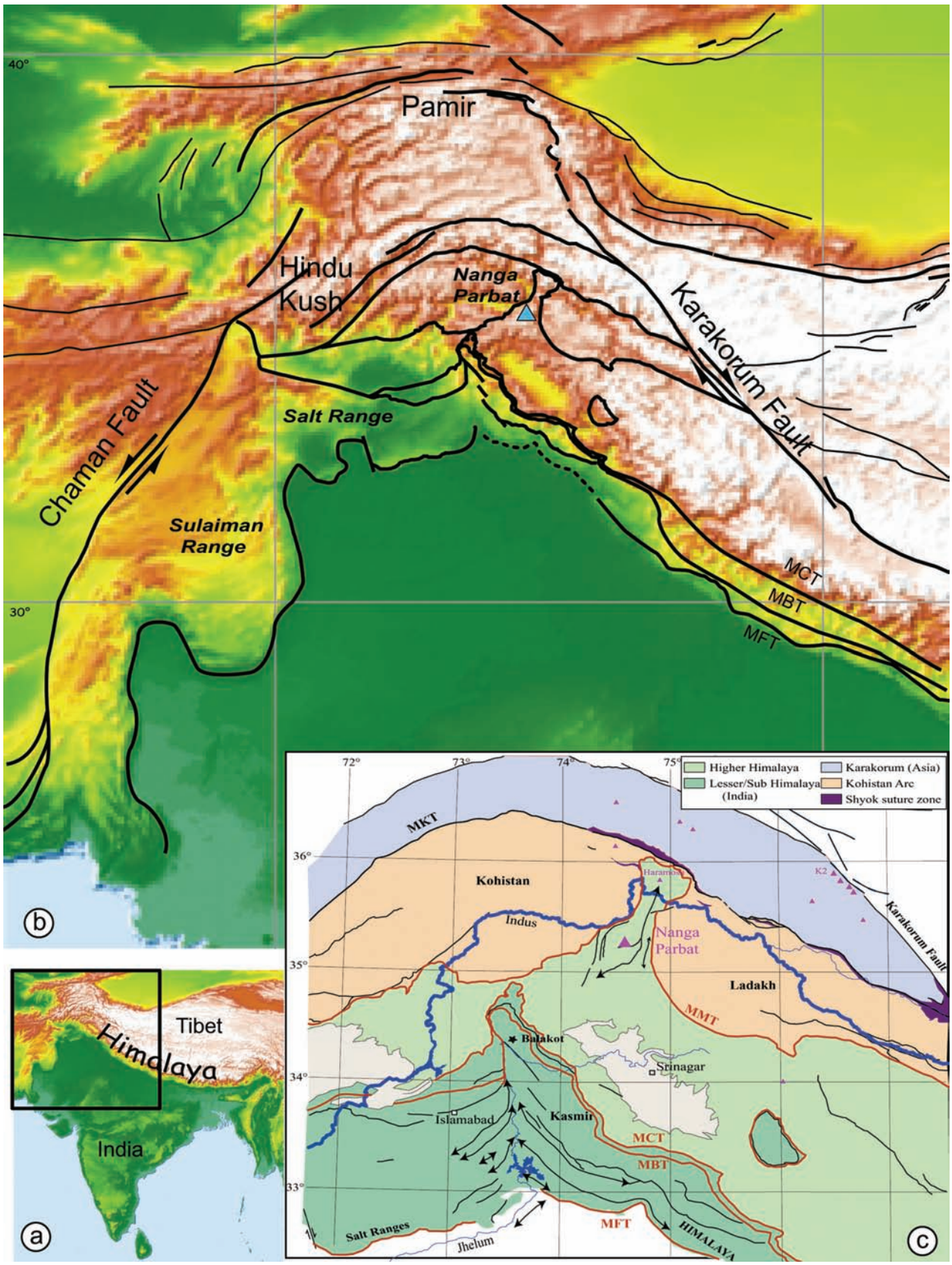

forms a prominent antiformal shape, compatible with the folding phase, and shows east–west extensional focal mechanisms, compatible with the recent extension phase (Meltzer *et al.* 2001). The Kashmir syntaxis is more complex. Its cartographic shape shows two directions of folding of the Miocene Siwaliks sandstone. The fold axes trend north–south along the Jhelum River, south of Balakot and provide evidence for post-Miocene east–west shortening (Coward *et al.* 1987; Figure 1). East of the Jhelum river, along the eastern border of the syntaxis, the trend of the fold axes change to NW–SE. Earthquake focal mechanisms indicate that NE–SW shortening still occurs in the Kashmir syntaxis, including the 2005 Balakot $M = 7.6$ event (Avouac *et al.* 2006). Both syntaxes belong to two distinct structural blocks, separated by the MCT, and are characterised by distinct deformation timing and trends of deformation.

The presence of the syntaxes reveals a component of east–west shortening during the north–south convergence of Indian with Asia. In this paper, we analyse the influence of the large-scale geometry of the NW Himalayan syntaxis, bordered by two strike-slip faults oblique to the convergence, specifically on the appearance of this east–west shortening component.

Sandbox experiments to investigate the evolution of a sedimentary accretionary wedge like that in the Himalayas (e.g. Malavieille 1984; Mulugeta & Koyi 1987; Mugnier *et al.* 1997; Smit *et al.* 2003) used dry sand or microbeads as analogues for natural brittle rocks (e.g. Hubbert 1937). Attempts to investigate the curvature of a wedge, as observed for the Himalayan wedge, have used indenters with a curved shape to create curved thrust wedges, inferring possible warping of the Indian slab at depth (Marshak 2004; Schellart & Lister 2005). Other models to reproduce the specific geometries of the NW Himalayan syntaxis have used multiple techniques. For example, the Sulaiman Range in Pakistan (Figure 1) has been modelled: (1) as a transfer zone between one fast and one slow indenter (Reiter *et al.* 2011); (2) by lateral variation in the rheology (Cotton & Koyi 2000); (3) as moving block along the Chaman Fault (Haq & Davis 1997). These experiments reproduced the salient shape of the Sulaiman range, by imposing lateral variations on the size of the structure. In this paper, we test the influence of the large-scale geometry of the NW Himalayan syntaxis on the construction of a wedge. We constructed a sandbox with two oblique edges representing, to the west, the Chaman Fault and, to the east, the Karakorum Fault (Figure 1c). The aim of this experimental set-up is to test if the presence of the oblique edges can generate east–west shortening in a north–south convergence, and if this east–west shortening could generate small-scale syntaxes like the Nanga Parbat.

EXPERIMENTAL SET-UP

In order to analyse the deformation of a standard analogue brittle crustal layer that shortens between two converging edges we chose to focus only on the influence of the two oblique edges. We did not try to reproduce the high structural and geological variability of the NW Himalayan syntaxis larger region. We did not reproduce the variability of the NW Himalayan Moho and Indian intracrustal decollement depth, or the presence of salt along the decollement to the west of the NW Himalayan syntaxis, beneath the salt ranges (Figure 1), and the absence of salt to the east. The localisation of the two main syntaxes appears independent both of the presence of salt, as the Kashmir syntaxis is close to the salt decollement but not the Nanga Parbat one, and of the decollement depth, shallow for the Kashmir syntaxis, deep for the Nanga Parbat one. We used a horizontal basal level. We focus on the brittle upper crust and used standard brittle materials, sand and microbeads (e.g. Malavieille 1984). On the contrary, we tested north–south difference of crustal thickness, which appears to be a more important parameter as it mimics the thin and soft Asia to the north and the thick and stiff cratonic India to the south. Both syntaxes belong to two distinct blocks, separated by the MCT, and are characterised by distinct deformation-phase timing and trend of deformation.

Experimental box and materials

The experimental set-up consisted of a rigid horizontal plate on which a mylar sheet is located (Figure 2). This sheet was pulled beneath a rigid backstop. We used standard analogue materials, including sand and microbeads (see complete description of these materials and variability in Schreurs *et al.* 2006). The sand is well-sorted quartz sand with a grain size of about 150 μm (Fontainebleau sand BR36, D50 = 151 μm, density 1.5 g/cm^3, angle of friction about 30°). The basal friction along the sand–mylar interface is about 20°. We also used glass microbeads (grain size 150 μm, friction angle 20°). Values for the angle of internal friction are generally

Figure 1 (a) Topography of the collision zone of India with Asia. (b) Large-scale NW Himalayan syntaxis, bounded to the west by the Chaman Fault, to the east by the Karakorum Fault and to the north by the subduction of Asian lithosphere beneath the Pamir. The shape is convex to the south. Two main small-scale syntaxes are observed, the Nanga Parbat and the Kashmir syntaxes. (c) From north to south, different continental crusts have been thickened during the collision; the thinner and softer Asian crust north of the suture (in blue north of the MKT); the Kohistan Volcanic Arc (in light orange) south of the suture; thick and stiff cratonic India more to the south. Three main thrusts accommodated the stacking of Indian crust: the MCT, which brings the Higher Himalayan Crystalline Massifs onto the Lesser Himalaya; the MBT, along which the Lesser Himalaya overrides the Siwalik Miocene detrital series; and the MFT between the Siwaliks and the Plio–Quaternary deposits of the foreland plain. Double black arrows show fold axes NNE–SSW in the Nanga Parbat syntaxis, and NNW–SSE in the western Kashmir syntaxis, compatible with a compression nearly east–west in the geodynamic context of the north–south convergence between India and Asia. Black star: 2005 Balakot $M = 7.6$ event.

comparable to those determined experimentally for upper crustal rocks (Byerlee 1978). Experimental modellers have long assumed that sand deforms according to the Coulomb failure criterion with constant frictional properties (e.g. Davis *et al.* 1983). More recent studies demonstrate that the mechanical behaviour of materials such as quartz sand and glass microbeads is more complex but very similar to the one exhibited by experimentally deformed rocks (Schellart 2000; Lohrmann *et al.* 2003).

Analogue models representing upper-crustal conditions can be scaled up to natural dimensions by observing geometric, kinematic and dynamic similarity relationships (Hubbert 1937). Scaling is such that 1 cm in the sandbox experiment is equivalent to 20 km in nature (size of the syntaxis about 1600 km in the east–west direction, size of the box 80 cm). The thickness of the sand layer is 1.5 cm, corresponding to 30 km, the mean thickness of the continental crust.

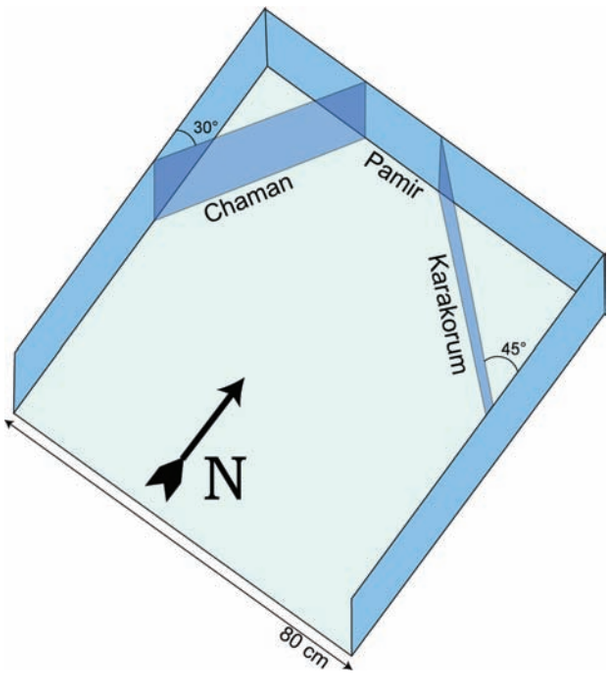

Figure 2 Sandbox geometry. The two oblique edges represent, to the west, the Chaman Fault making an angle of 30° with the western edge, and, to the east, the Karakorum Fault making an angle of 45° with the eastern edge. The box is 80 cm wide.

Completed models

We completed 25 experiments to model the deformation of a standard analogue brittle crustal layer converging between two edges oblique to the convergence. We used various materials: sand only, sand and microbeads at the base of the sand layer, or silicone putty at the base. We used various box geometries, including symetric or assymetric oblique edges or rectangular edges. We used thickness discontinuity, east and west or north and south. We present here the 8 most representative experiments (Table 1). These include experiments with the assymetric oblique edges (Figure 2) and associated rectangular benchmarks (JK1 & JK4). We discuss experiments with sand only (JK2), with a $\sim$2 mm microbeads layer at the sand base (JK3), and with microbeads along the oblique edges (JK7 & JK8; microbeads were supported vertically along the border by a paper sheet until the sand cover was installed, then the paper sheet is removed). Microbeads decrease the friction at the base of the sand layer or along the oblique edges (Schellart 2000; Schreurs *et al.* 2006), which allowed us to measure the variability of the east–west shortening due to variation of basal and side friction.

We used a constant thickness of the sand layer, scaled to the mean thickness of the continental crust, except for two experiments where the thickness of the sand layer is thicker on the southern half of the box (JK15 & 16). We tested the influence of a north–south crustal discontinuity that may be a key parameter for the localisation of the east–west shortening.

In this paper, we do not address the influence of the ductile salt layer of the salt range (Figure 1), not adequately modelled by sand, as we focus on the influence of the large-scale geometry with oblique edges.

BENCHMARK EXPERIMENTS AND METHODS

We compared parameters on a benchmark model in a rectangular box with parameters in an oblique edges box. It has been shown that the reproducibility of such experiments depends on the material used in each laboratory (Schreurs *et al.* 2006). We also present the methods used to determine the displacement field.

Table 1 Geometric parameters of the different experiments.

Experiment	Box geometry	Sand thickness	Microbead	Wedge propagation (%)	East–west shortening (%)
JK 01	Rectangular (benchmark)	1.5 cm equivalent	None	97	
JK 04		to mean crustal thickness	Base	116	
JK 02	Oblique edges		None	88	38
JK 03			Base	108	32
JK 08			Edges	95	41
JK 07			Base + edges	139	32
JK 15		15 cm north	Base		
JK 16		2 cm south	None (?)		

Benchmark with sand, rectangular box (JK1)

With only sand (JK1), forward propagation of 6 thrusts for 20 cm of convergence (Figure 3a) occurred with some minor back-thrusts also visible. The propagation of the wedge is 97% of the total convergence (measured between first and last pictures of the experiment). Each new thrust initiated every 3–4 cm of convergence (1–2 cm, 3–4 cm, 8–9 cm, 12–13 cm, 16 cm, 18–19 cm). The distance between one new fault and the front is between 4.5 and 6 cm, which is three to four times the thickness of sand layer.

In cross-section, the first order structure is rather simple, with a major forward thrust corresponding to each fold (Figure 3a). In detail, the structure is more complex, with several minor backthrusts, some of which affect the surface. The dip of frontal part of the wedge is about 8° (frontal-imbrication zone in Lohrmann *et al.* 2003). Close to the backstop, the top of the wedge is horizontal and the length of this horizontal part is 3.6 cm (internal-accumulation zone in Lohrmann *et al.* 2003). It shows that the critical-taper analysis of wedges must be restricted to the frontal segment.

The parameters measured for this benchmark experiment, such as the north–south length of the wedge, are compared with same parameters obtained with oblique edges.

Method to determine the displacement field

The displacement field is measured for the last increment of the experiment, using the pictures of 18 and 20 cm steps of convergence (Figure 3a). We used the Cosi-Corr plug into ENVI software, made for sub-pixel correlation of satellite images (Leprince *et al.* 2007; Ayoub *et al.* 2009) to study ground deformation (e.g. Avouac *et al.* 2006). This plugin correlates one pixel of the picture of step n with one pixel of the picture of step $n + 1$. The result is the displacement field between both steps. We used Cosi-Corr frequency parameters of 128 pixels for the initial Window size (size of initial search zone around the pixel considered), 16 pixels for the final Window size, and 4 pixels for step (one measurement each 4 pixels of the picture; for more details on these parameters see Leprince *et al.* 2007 and Ayoub *et al.* 2009). These automatic measurements (blue arrows, Figure 3a) compared well with measurements made by correlating one pixel of the picture of step n with one pixel of the picture of step $n + 1$ by hand (black arrows). For the other experiments, only the automatic measurements were used, which are faster and homogeneous across the picture.

Between JK1 frontal thrust 6 and 5, the displacement is 56% of the undeformed sand displacement (southern blue arrows), then it decreases to the north, 24% between thrusts 5 and 4, 15% between thrusts 4 and 3, and 6–7% between thrusts 3 and 1. We deduced the displacement rate of each fault by subtracting the two displacement vectors on both side of the fault: the rate decreases from 44% of the convergence rate (southern blue arrows) for the frontal thrust, to 32%, 12%, 8% then 1% for the northern one (Figure 3a). Each fault is continuously active throughout the experiment.

Benchmark with glass microbeads at the base, rectangular box (JK4)

With microbeads at the base of the sand layer (JK4), the final model is quite similar to JK1, although the thrusts are more regular (Figure 3c). In cross-section, a major forward thrust is observed for each fold, and few minor backthrusts occur, mainly reaching the surface close to the forward thrust. The dip of the wedge is about 5° (Figure 3d). The horizontal portion of the wedge close to the backstop is wider than for JK1 (length 8.8 cm).

We observed seven to eight thrusts over 20 cm of convergence (two more thrusts than for JK1). The propagation of the wedge is 116% of the total convergence,

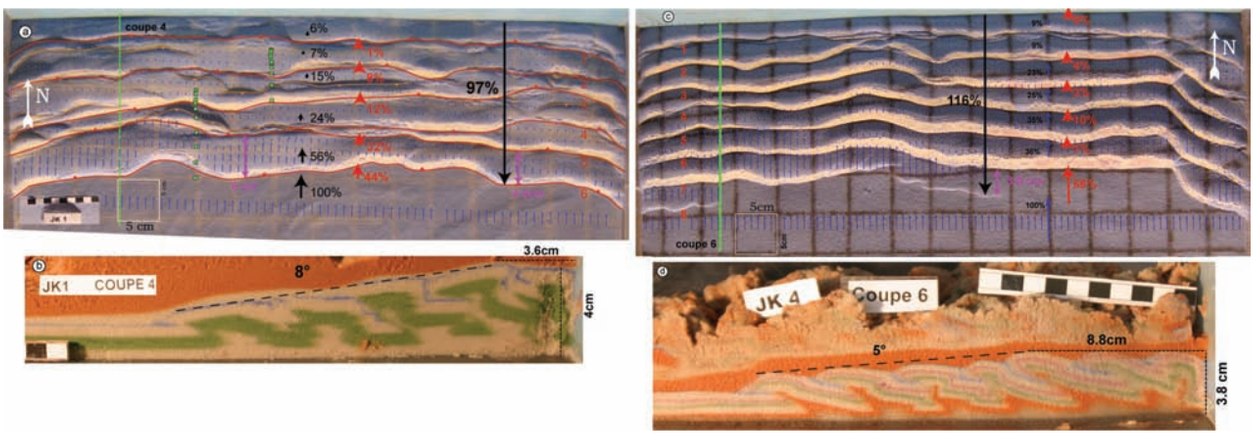

Figure 3 (a) JK1 benchmark experiment with only sand, 1.5 cm thick. The box is 80 cm wide, gridded each 5 cm (white square). The convergence is 20 cm. Red lines: major thrusts; orange lines: minor backthrusts; large black arrow: propagation of the wedge (97% of the total convergence); small black arrows: displacement vectors determined manually between 18 and 20 cm of convergence; small blue arrows: displacement vectors determined by Cosi-Corr (Leprince *et al.* 2007; Ayoub *et al.* 2009); red arrows: thrust rate compare to the convergence rate; green squares: successive position of one point each 2 cm of convergence. (b) Cross-section of JK1. (c) JK4 benchmark experiment with glass microbeads at the base of the sand layer, large blue arrows: same as small ones, enlarged three times. (d) Cross-section of JK4.

about 20% more than for JK1. A new thrust initiated every 2–3 cm of convergence. The distance between one new fault and the front is about 4 cm, slightly less than for JK1. The effect of microbeads at the base is to propagate the deformation further, with thrusts that initiate more regularly, more often and closer to each other than for the experiment with sand only (JK1).

During the last increment of the experiment, between 18 and 20 cm of convergence, the displacement field has been estimated using Cosi-Corr. The displacement is only 36% of the undeformed sand displacement between frontal thrust and thrust 5. This indicates that the frontal thrust rate is 68% of the convergence rate, 24% more that for JK1. Thrust 5 north of the frontal thrust appears inactive, but thrusts north of it have a rate between 10 and 2% of the convergence rate.

DISPLACEMENT FIELD WITHIN A DOUBLE OBLIQUE CONVERGENCE

We added to the rectangular box two oblique edges (Figure 2). The aim of this experimental set-up is to investigate the structural evolution of a standard analogue brittle crustal layer during a north–south convergence in response to the influence of the two oblique edges. We analysed the structures in two and three dimensions, the evolution in space of the deformation field induced, and the amount of material transfer along the borders.

Double oblique convergence with glass microbeads at the base, JK3

We first analysed the experiment with the microbeads at the base (JK3). After 4 cm of convergence, one continuous thrust appeared along the 3 borders of the box (Figure 4). The distance between each thrust is smaller along the western box border, making a lower angle with the convergence vector than the eastern border. A second thrust initiated along the western border of the box, and ended at its NE corner. After 8 cm of convergence, the second thrust propagated along the whole eastern border. A third thrust propagated from the SW corner, along the western border and stopped at the NE corner. After 12 cm of convergence, a fourth thrust propagated in the opposite direction (from SE corner, along the eastern border). After 16 cm of convergence, the alternation of thrusts from one southern corner to the opposite northern corner continued.

Along the oblique borders, the material migrated tangentially toward the north of the box, while along the northern border perpendicular to the convergence, the material migrated orthogonally to the border (green square, Figure 5a). To quantify precisely the motion of the material, we used the displacement field obtained using Cosi-Corr (frequency parameters 64-16–4). We decomposed one displacement vector (purple arrow, Figure 5b) into 2 vectors, one parallel to the border (purple number), one perpendicular to it (black number) and substracted the two components on each side of one fault to estimate the corresponding components on the fault (compression component is light red arrow orthogonal to the oblique edges; strike-slip component is dark red arrow parallel to the oblique edges).

As in the rectangular experiment JK4 (Figure 3), the compression component is absorbed mainly by the frontal thrust (between 48 and 60% of the compressional component of convergence, light red arrow and numbers Figure 5). As in JK4, the western border shows a small compressional component for thrust number 4 (6–10%), then an increase for thrust number 3 (19%), and a decrease for thrusts number 2 and 1 (2%). On the eastern and northern borders, the compressional component decreases to the north, 30–36% on thrust 4, 1–4% for thrusts 1, 2 and 3.

The strike-slip component (dark red arrow and number, Figure 5b) follows approximately the same distribution as the compressional one. On the eastern side, it is mainly absorbed by the frontal thrust and thrust 4. On the western side, the strike-slip component is mainly absorbed on the frontal thrust in the middle of the border, but more distributed on thrusts 3, 4 and 5 to the south. A part of this strike-slip motion is absorbed on small back thrusts (orange lines, Figure 5b). The angle between the displacement vector and the edge (α, Figure 5b) decreases from the front toward the border, indicating that the strike-slip component increases with respect to the compressional one from the front toward the border. This angle increases toward the north indicating that the strike-slip component decreases toward north relative to the compressional one.

The wedge slope is similar to the rectangular experiment JK4, about 5°, on the southern part of the cross-section. It increases close to the oblique edges. Close to the northern edge, the length of the plateau increased a little compared to JK4 (Figure 5c).

Double oblique convergence with only sand, JK2

With only sand (JK2), the evolution of the fault pattern is very similar to JK3, with the propagation by alternation of thrusts from one southern corner to the opposite northern corner (Figure 6e). Cross-sections perpendicular to the oblique borders show that the equilibrium of the wedge is perturbed by the oblique motion (Figure 6f–h). Close to the front, the equilibrium slope is similar to the slope measures in the sand rectangular experiment JK1, 7–8° (Figure 2b); close to the borders, the slope is greater. Along the northern border, the flat plateau length (7.2 cm; Figure 6g) doubles compared to JK1 (Figure 2b).

As in JK3, the material migrated tangentially along the oblique borders, while the material migrated perpendicularly to the northern border (green squares, Figure 6e). We could not measure the displacement field in this experiment precisely, as the sand surface had been too perturbed by material sliding along the oblique borders (Figure 6e).

After 9 cm of convergence, we observed the formation of two folds at the junction between the oblique and perpendicular borders, with axes perpendicular

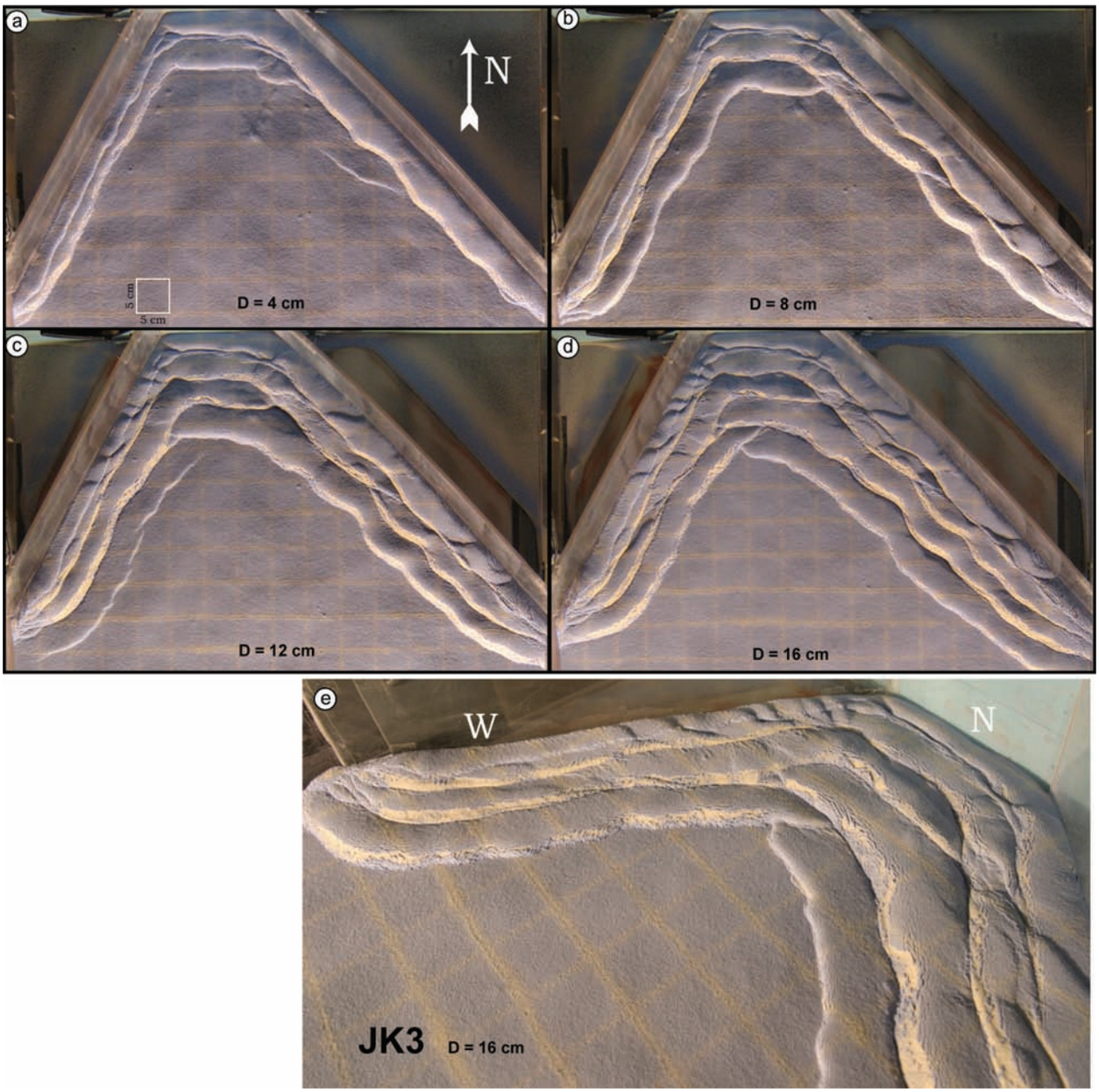

Figure 4 JK3, oblique edge experiment with microbeads at the base of the sand layer (1.5 cm thick); four successive steps at 4, 8, 12 and 16 cm of convergence. Side view of step 16 cm.

to the oblique borders (indicated by red double arrows, Figure 6d, e).

EAST–WEST SHORTENING VARIATION OWING TO VARIATION IN BASAL AND SIDE FRICTION

To increase the strike-slip component along the borders, we added some glass microbeads. One experiment used only sand except along the oblique edges (JK8), and one with microbeads at the base and along the oblique edges (JK7). The propagation distance is smaller than the total convergence for both experiments with only sand at the base, but increases with the micro-beads along the borders (88% for JK2 <95% for JK8, both <100%; Figure 7a and c). With microbeads at the base, the propagation distance is greater than the total convergence, and increases with the micro-beads along the border (108% for JK3 <139% for JK7, both >100%; Figure 7b, d).

With the microbeads along the borders, the angle increases between the east and west frontal thrusts (syntaxis angle). To visualise this effect, we draw black dotted lines on Figure 7 parallel to the edges close to the frontal thrusts. For JK2 and JK3, without microbeads along the edges, this black dotted line is almost parallel to the frontal thrusts (Figure 7a, b). For JK7 and JK8, with microbeads along the edges, the angle between this black dotted line and the frontal thrusts increases (Figure 7c, d). The increase of the syntaxis angle resorbs

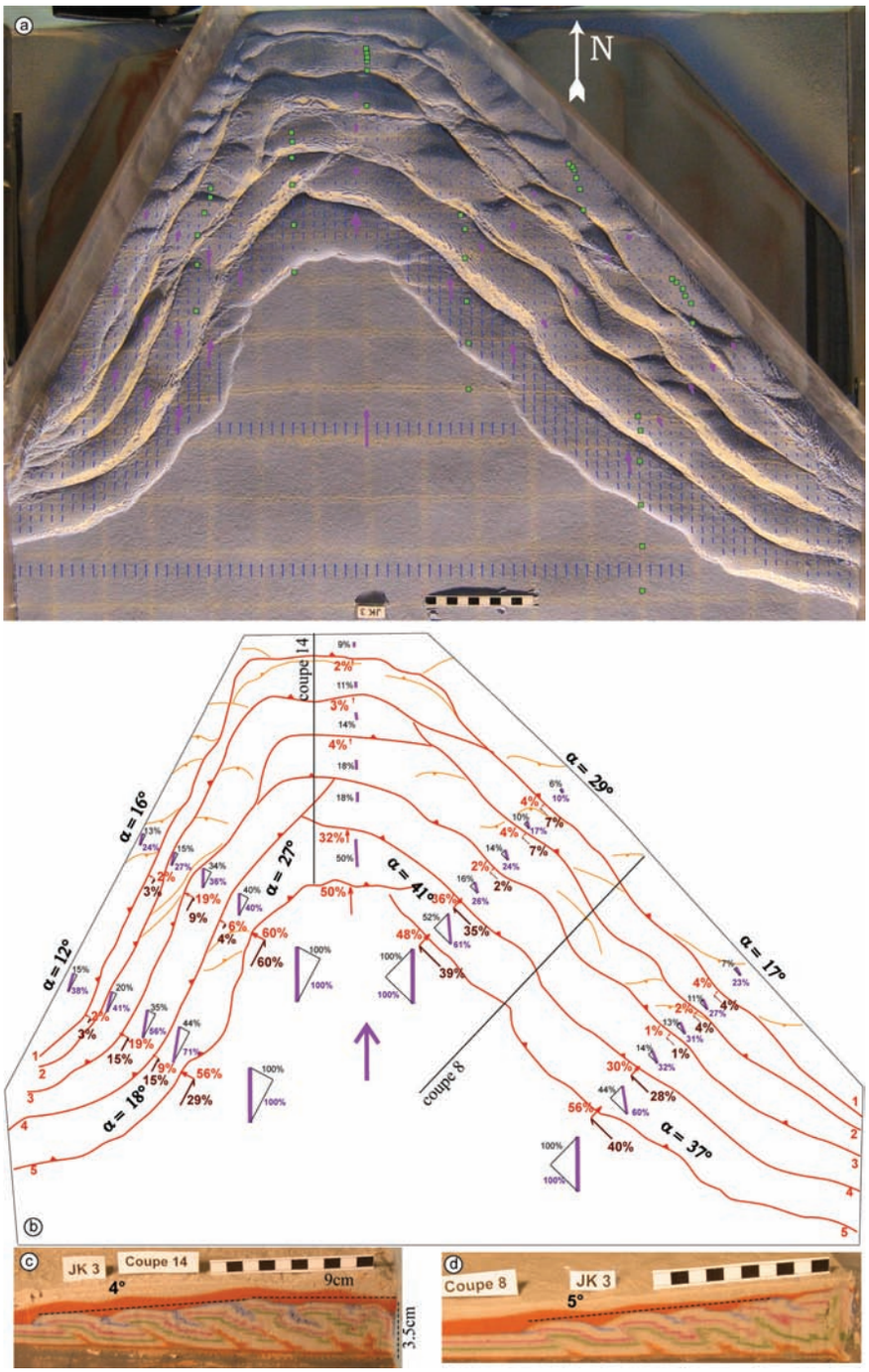

Figure 5 JK3 (a) displacement field using Cosi-Corr, see legend of Figure 3, and (b) decomposition of displacement vector (purple line) into two vectors, one parallel to the border (purple number), one perpendicular to it (black number). Light red arrows and numbers: compressional component of the fault, compared with convergence vector compressional component; dark red arrows and numbers: strike-slip component compared with convergence vector strike-slip component.

the syntaxis geometry for JK8 and JK7 (if the angle increases more it could cancel the syntaxis geometry making one continuous east–west trending frontal thrust).

We also measured the offset of north–south lines of the grid by successive faults (Figure 7), and compared this offset to the total convergence (value in percent). From north to south, the offset increases southward to the middle of the oblique border, then decreases northward. The maximum east–west shortening is obtained by adding the maximum value of this offset on each side. For example, for JK2 the maximum east–west offset is 20% to the west (light blue north–south line), 18% to the east (light pink north–south line), making the maximum east–west shortening for JK2 of 38%. The east–west shortening is 32% for JK3 and JK7, and 41% of the convergence for JK8. The two experiments with microbeads at the base (JK3, JK7) show the smallest values (32%). For the experiments with sand at the base, values are higher, 38% for JK2 with only sand, which increases to 41% for JK8 with microbeads along the edges.

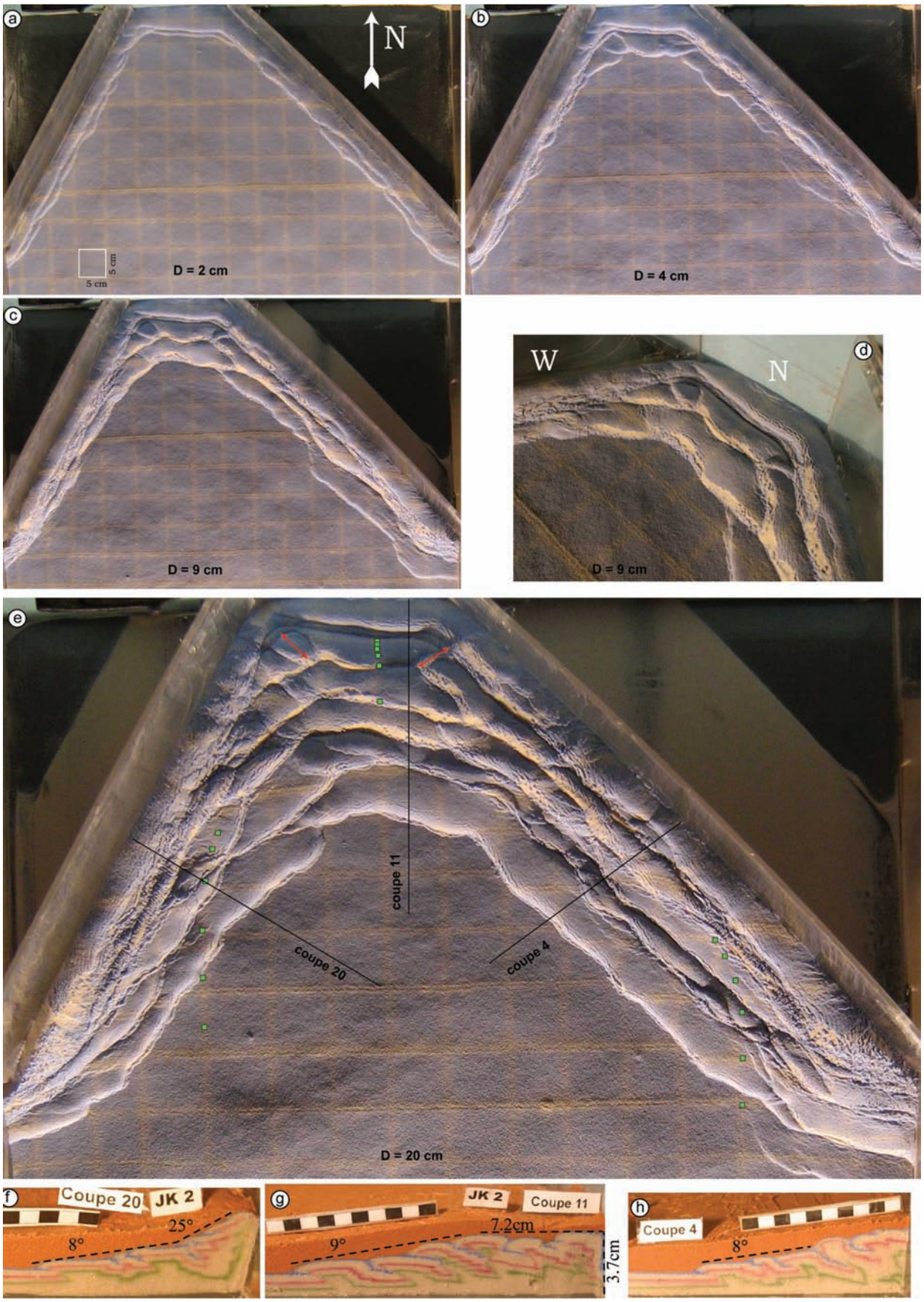

Figure 6 JK2, oblique edge experiment with only sand (1.5 cm thick); three successive steps at 2, 4 and 9 cm of convergence. Side view of step 9 cm, showing two folds perpendicular to the oblique edge (red arrows).

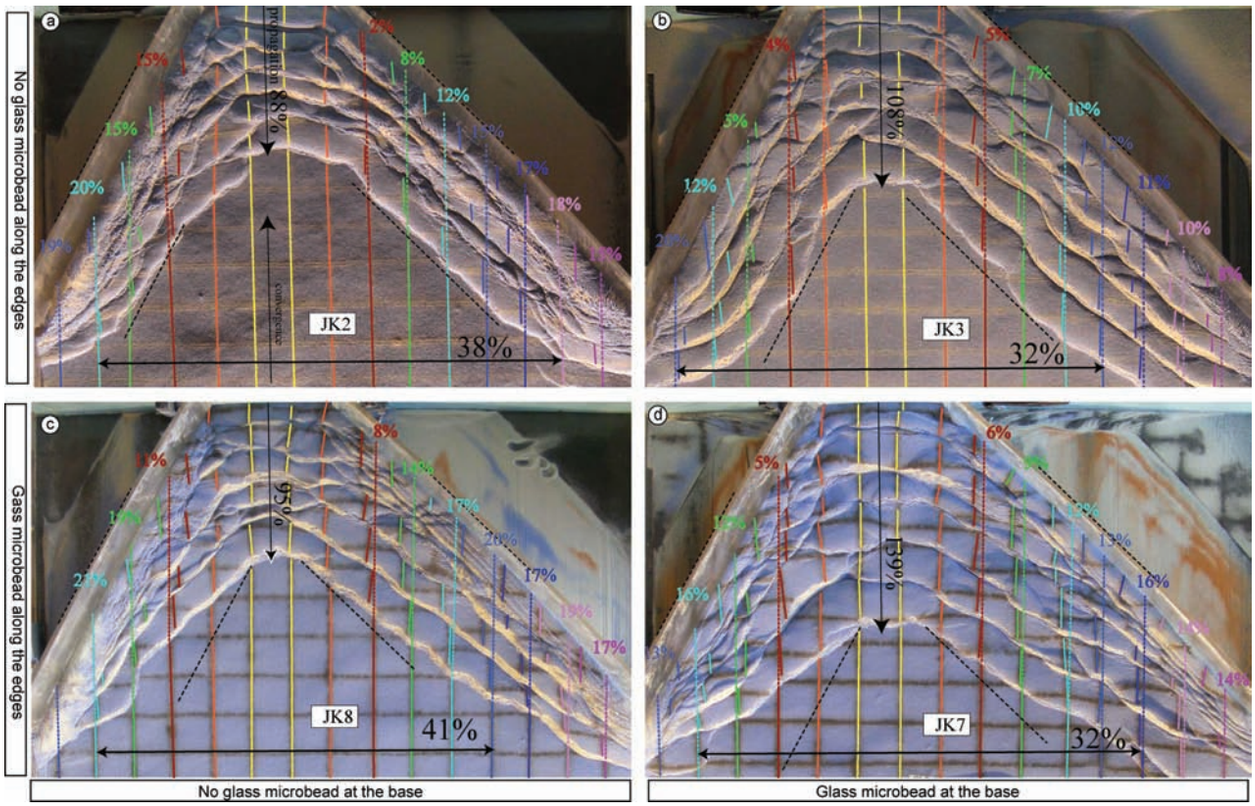

Figure 7 Comparison of experiments with variation of basal and side friction: JK2 sand only, JK3 microbeads at the base, JK8 microbeads along the edges, JK7 microbeads at the base and along the edges. Offset of north–south lines (one colour each, with offset value) of the grid by successive faults. East–west black arrow: maximum east–west shortening. Arrow to the south, propagation of the wedge; arrow to the north, convergence. Black dotted lines parallel to the edge parallel the frontal thrusts for JK2 and JK3, without microbeads along the edges. For JK7 and JK8, with microbeads along the edges, the angle between black dotted line and frontal thrusts increases, which resorbs the syntaxis geometry (if the angle increases more it could cancelled the syntaxis geometry making one continuous frontal thrust east–west).

INFLUENCE OF THICKNESS DISCONTINUITY

Formation of a plateau, JK16

The influence of a north–south discontinuity within the sand thickness was tested by placing a 1.5 cm thick sand layer to the north of the box (in green on Figure 8), and a 2 cm thick layer to the south of the box (in blue). In this experiment, the thinner crust deformed until reaching a flat plateau, before the thicker crust began to deform (Figure 8). The slope of the wedge perpendicular to the north border is dichotomous, with two flat portions separated by a sharp topographic step, one at high altitude to the north, one undeformed at low altitude to the south. This experiment reflects the influence of a north–south thickness discontinuity, effectively compartmentalising deformation.

Formation of north–south axis fold within a north–south convergence, JK15

As for experiment JK16, there is a 1.5 cm thick sand layer below the northern green part of the box, and a 2 cm thick layer below the southern blue part. We did not deposit sand in the southern part of the box, which therefore acted as a free edge (JK15; Figure 9). The fault pattern in the thick blue southern portion is remarkable, as faults with trend different from the edges of the box, appeared within the sand layer. Strike-slip faults trending NE–SW occur to the east of the box, and NW–SE-trending faults to the west (red arrow, Figure 9). These strike-slip faults bound blocks that rotate anticlockwise in the east and clockwise in the west (rotation of black grid clearly visible on Figure 9). In the middle of the box, we observed a fold with an axis trending north–south (black double-arrow, Figure 9). In cross-section, it is bounded by two antithetic reverse faults, forming a pop-up fold. Between the north and the south of the thick blue block, strike-slip faults are orthogonal to each other. They are conjugated to orthogonal thrust faults, with the north–south fold terminated to the north along an east–west thrust (Figure 9).

The consequence of the free southern boundary condition is the appearance of pure strike-slip faults within the sand layer that are conjugated to pure shortening on one north–south fold. This experiment shows that pure strike-slip motion on the borders could generate a north–south trending fold in the center during a north–south convergence. The east–west shortening generated by the edges oblique to the

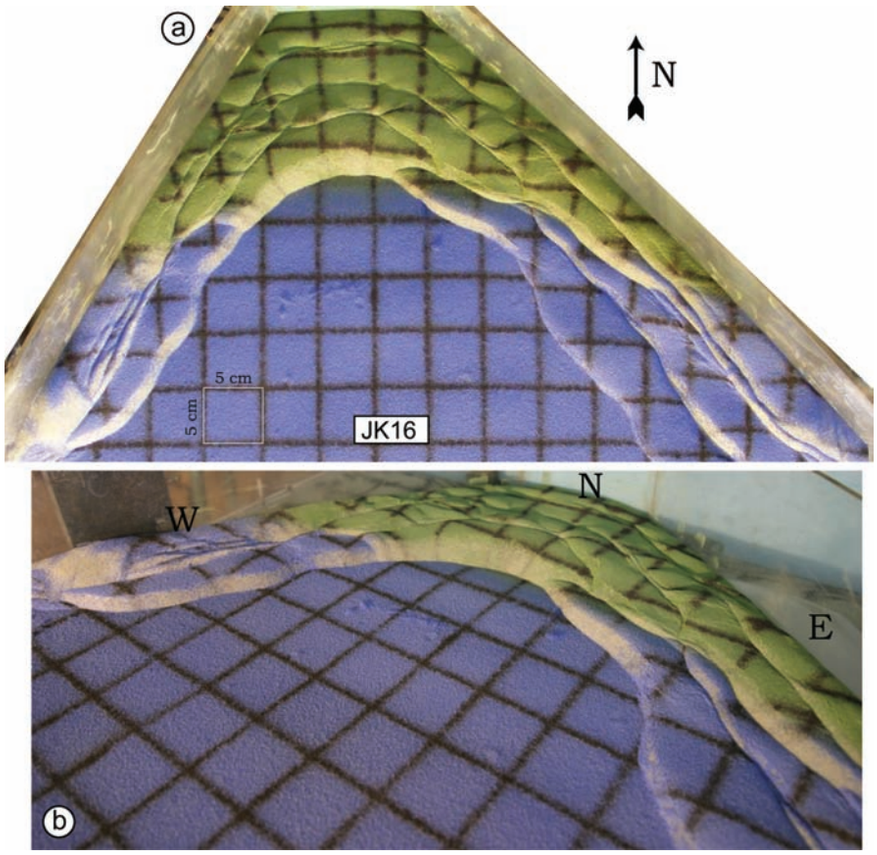

Figure 8 JK16: discontinuity within the sand thickness: 1.5 cm thick sand to the north of the box (in green), 2 cm to the south (in blue). Convergence = 15 cm.

north–south convergence is absorbed by a north–south trending fold when partitioning occurs with pure strike-slip faults.

DISCUSSION: HOW TO ABSORB EAST–WEST SHORTENING DURING NORTH–SOUTH CONVERGENCE?

We modelled the convergence of a standard analogue brittle crustal layer between two edges oblique to the convergence. This experimental set-up shows that the obliquity of the edges can generate east–west shortening during north–south convergence. The quantitative analyse of the experiments shows that the east–west shortening is coupled to the forward propagation of the wedge. Variations in the friction at the base or along the oblique edges modified the balance between these two kinematic processes (Figure 7).

Adding oblique edges to the rectangular box retards the forward propagation of the wedge. Wedge propagation in the rectangular box with sand only (JK1) makes up 97% of the total convergence, but only 88% with oblique borders (JK2). It also decreases with microbeads at the base, 116% for the rectangular box (JK4), and only 108% with oblique borders (JK3). The oblique edges introduced a strike-slip component of motion, which changed the equilibrium of the wedge. Close to the oblique edges, the slope is steeper (see cross-sections on Figures 5, 6). Close to the northern border of the box, the flat portion of the wedge is wider in the oblique box than in rectangular box. More material is stored close to the edges, and the propagation of the wedge decreases. One experiment (JK 16) shows an extreme case of a flat plateau on the whole northern portion of the box, if the sand layer is thinner to the north (Figure 8).

Among the oblique experiments, when the strike-slip component increases by adding some microbeads along the edges that decreases the friction, both mechanisms (east–west shortening and forward propagation of the wedge) could absorb the convergence. Comparing JK2, with only sand, and JK8, with microbeads only along the edges, both the propagation of the wedge and the east–west shortening increase (Figure 7a, c). But comparing JK3, with microbeads at the base, and JK7, with microbeads also along the edges, only the propagation of the wedge increases. Experiment JK7 is the only case where the forward propagation of the wedge is wider than the rectangular experiment, about 140% of the convergence (Figure 7d). Another clear effect of the increase in the strike-slip motion with microbeads along the edges, is to widen the angle between both sides of the syntaxis, which tends to resorb the geometry (if the syntaxis angle increases more it could make one continuous frontal thrust east–west and cancel the syntaxis geometry; JK7 and JK8 on Figure 7c, d). With no microbeads along the edges, the angle is similar after 20 cm of convergence (JK2 and JK3, Figure 7a, b). Only one experiment, JK15, shows a lowering of the syntaxis angle, with successive strike-slip faults migrating toward the

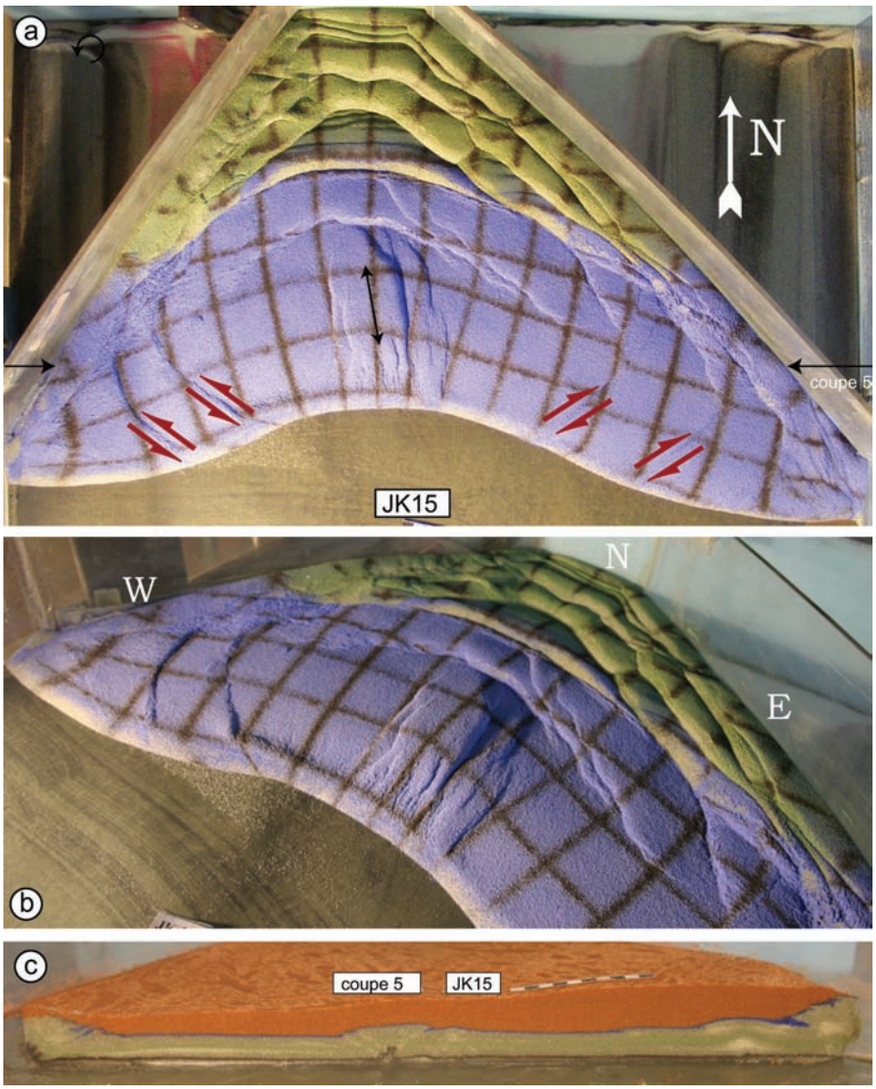

Figure 9 JK15 discontinuity within the sand thickness: 1.5 cm thick sand to the north of the box (in green), 2 cm to the south (in blue). No sand to the south of the box, which acted like a free boundary. Experiment showing partitioning of the deformation: red arrow showing strike-slip fault; black arrow showing north–south fold. Convergence = 80 cm.

center of the box (Figure 9). This closure of the syntaxis is associated with a north–south trending fold, in the middle of the box. We conclude that the amount of strike-slip motion is not critical to the formation of north–south folds and that the increase of strike-slip motion could be absorbed by the propagation of the wedge, with the widening on the syntaxis angle. The lowering of the syntaxis angle appears to be a critical parameter.

The oblique edges of the box generated up to 40% of east–west shortening, compared to the total north–south convergence (Figure 7). In these experiments, the east–west shortening is accommodated by oblique motion on transpressive faults parallel to the edges, with up to 60% of strike-slip component, compared to the convergence vector (Figure 5). There is no formation of one singular structure that accommodated the east–west shortening. Some folds formed perpendicular to the edges in two experiments JK2 (Figure 6d) and JK7, but they did not evolve in to major structures that accommodated some convergence. One experiment (JK15) showed one north–south trending fold, parallel to the convergence vector, which absorbs the east–west shortening component (Figure 9). The consequence of the free southern boundary condition of experiment JK15 is the appearance of pure strike-slip faults within the sand layer, conjugated to pure shortening on one north–south fold. We conclude that the obliquity of the edges compared to the convergence vector leads to the appearance of a shortening component perpendicular to the convergence vector, which could be absorbed on a fold parallel to the convergence vector.

The similarity of experimental-box geometry with the large-scale geometry of the NW Himalayan syntaxis allows some comparison of our model to the NW syntaxis (Figure 1).

Two experiments show that the consequence of a north–south thickness discontinuity is distinct evolution of both areas (Figures 8, 9). This dichotomy between blocks is also observed at the scale of the NW Himalayan syntaxis, where large blocks with different rheology are characterised by distinct deformation-phase timing and trends of deformation (Pêcher *et al.* 2008; Figure 1). The two main syntaxes belong to two distinct blocks and are characterised by distinct trends of deformation separated by a main

Himalayan thrust (the MCT; Figure 1). At the scale of the Asia/India collision, soft Asia deforms widely to the north, forming the flat and high Tibetan Plateau, while a part of India remains flat and underformed to the south.

In the NW syntaxis, the small-scale syntaxes such as the Nanga Parbat, reveal a component of east–west shortening during the north–south convergence of India with Asia. Our experiments show that the two faults oblique to the convergence bordering the NW Himalayan syntaxis, generated an east–west shortening component. This east–west component was absorbed either by transpressive motion on faults parallel to the edges, if the motion on the edges is transpressive, or by a north–south-trending fold, if the motion on the edges is pure strike-slip. In our experimental set-up, the oblique edges did not act as strike-slip faults, but as transpressive faults. The shortening component perpendicular to the convergence vector was absorbed by transpressive motion. In the NW Himalayan syntaxis, the Chaman and Karakorum Faults act as strike-slip faults, which could generate a north–south fold such as the Nanga Parbat to absorb the east–west shortening component. We conclude that the obliquity of the edges is sufficient to generate an east–west shortening component in a north–south convergence, but partitioning of the oblique motion is necessary to generate a north–south axial-trending fold such as the Nanga Parbat.

CONCLUSION

We modelled the large-scale NW Himalayan syntaxis geometry, bordered by the Chaman strike-slip Fault to the west and the Karakorum Fault to the east, using a sandbox with edges oblique to the convergence. We analysed the deformation of a standard analogue brittle crustal layer converging between two edges oblique to the convergence was analysed with a focus on the influence of the obliquity of the edges but did not try to reproduce the high structural and geological variability of the NW Himalayan syntaxis region. Our analysis shows that the obliquity of the edges can generate east–west shortening in a north–south convergence. We quantified up to 40% of the north–south convergence vector. The east–west shortening is accommodated by oblique motion on transpressive faults parallel to the edges, with up to 60% of a strike-slip component, compared to the convergence vector. One experiment, with a free southern boundary, shows pure strike-slip faults within the sand layer, conjugated to pure shortening on one north–south fold. We conclude that the obliquity of the edges is sufficient to generate an east–west shortening in a north–south convergence, but partitioning of the oblique motion is necessary to generate a north–south axial-trending fold.

In the NW syntaxis, the small-scale syntaxes like the Nanga Parbat reveal a component of east–west shortening during the north–south convergence of Indian with Asia. Our experiments show that both the obliquity to the convergence and the strike-slip motion of Chaman and Karakorum Faults acting as the NW Himalayan syntaxis borders could generate a north–south fold as the Nanga Parbat to absorb the east–west shortening component.

ACKNOWLEDGEMENTS

The experiments have been done at the Université de Toulouse, in the experimental laboratory of Francis Odonne, with the precious help of Nicole Guerrero. The project was supported with internal funding of the Université de Grenoble 1 Joseph Fourier (TUNES). We thank Arnaud Pêcher from fruitful discussions.

REFERENCES

Avouac J-P., Ayoub F., Leprince S., Konca O. & Helmberger D. V. 2006. The 2005, Mw 7.6 Kashmir earthquake: Sub-pixel correlation of ASTER images and seismic waveforms analysis. *Earth and Planetary Science Letters* **249**, 514–528.

Avouac J-P. & Tapponnier P. 1993. Kinematic model of active deformation in central Asia, *Geophysical Research Letter* **20**, 895–898.

Ayoub F., Leprince S. & Avouac J-P. 2009. Co-registration and correlation of aerial photographs for ground deformation measurements. *Journal of Photogrammetry and Remote Sensing* **64**, 551–560. doi:10.1016/j.isprsjprs.2009.03.005

Berger A., Jouanne F., Hassani R. & Mugnier J. L. 2004. Modelling the spatial distribution of present-day deformation in Nepal: how cylindrical is the Main Himalayan Thrust in Nepal? *Geophysics Journal International* **156**, 94–114. doi:10.1111/j.1365-246X.2004.02038.x

Burbank D. W. 1983. The chronology of intermontane-basin development in the northwestern Himalaya and the evolution of the Northwest Syntaxis. *Earth and Planetary Science Letters* **64**, 77–92.

Byerlee J. 1978. Friction of rocks. *Pure and Applied Geophysics* **116**, 615–626.

Cotton J. T. & Koyi H. A. 2000. Modeling of thrust fronts above ductile and frictional detachments: Application to structures in the Salt Range and Potwar Plateau, Pakistan. *Geological Society of America Bulletin* **112**, 351–363.

Coward M. P., Rex D. C., Asif Khan M., Windley B. F., Broughton R. D., Luff I. W., Petterson M. G. & Pudsey C. J. 1987. Collision tectonics in the NW Himalayas. *Geological Society, London, Special Publications* **19**, 203–219.

Davis D., Suppe J. & Dahlen F. A. 1983. Mechanics of fold-and-thrust belts and accretionary wedges. *Journal of Geophysical Research* **88**, 1153–1172.

Grelaud S., Sassi W., de Lamotte D. F., Jaswal T. & Roure F. 2002. Kinematics of eastern Salt Range and South Potwar Basin (Pakistan): a new scenario. *Marine and Petroleum Geology* **19**, 1127–1139. doi:10.1016/S0264-8172(02)00121-6

Haq S. S. B. & Davis D. M. 1997. Oblique convergence and the lobate mountain belts of western Pakistan. *Geology* **25**, 23–26.

Hubbert M. K. 1937. Theory of scale models as applied to the study of geologic structures. *Geological Society of America Bulletin* **48**, 1459–1519.

Leprince S., Barbot S., Ayoub F. & Avouac J-P. 2007. Automatic and precise orthorectification, coregistration, and subpixel correlation of satellite images application to ground deformation measurements, IEEE transactions on geoscience and remote sensing. *IEEE transactions on geoscience and remote sensing* **45**, 1529–1558. doi:10.1109/TGRS.2006

Lohrmann J., Kukowski N., Adam J. & Oncken O. 2003. The impact of analogue material properties on the geometry, kinematics, and dynamics of convergent sand wedges. *Journal of Structural Geology* **25**, 1691–1771.

Malavieille J. 1984. Modélisation expérimentale des chevauchements imbriqués: application aux chaînes de montagnes. *Bulletin de la Société Géologique de France* **26**, 129–138.

MARSHAK S. 2004. Salients, recesses, arcs, oroclines, and syntaxes; a review of ideas concerning the formation of mapview curves in fold-thrust belts. *In*: McClay K. R. ed. *Thrust tectonics and hydrocarbon systems. AAPG Memoir* **82**, 131–156.

MELTZER A., SARKER G., BEAUDOIN B., SEEBER L. & ARMBRUSTER J. 2001. Seismic characterization of an active metamorphic massif, Nanga Parbat, Pakistan, *Himalayan Geology* **29**, 651–654. doi:10.1130/0091-7613(2001)029<0651:SCOAAM>2.0.CO;2.

MUGNIER J. L., BABY P., COLLETTA B., VINOUR B., BALE P. & LETURMY P. 1997. Thrust geometry controlled by erosion and sedimentation: A view from analogue models. *Geology* **25**, 427–430.

MULUGETA G. & KOYI H.1987. Three-dimensional geometry and kinematics of experimental piggyback thrusting. *Geology* **15**, 1052–1056.

NEGREDO A. M., REPLUMAZ A., VILLASENOR A. & GUILLOT S. 2007. Modeling the evolution of continental subduction processes in the Pamir–Hindu Kush region. *Earth and Planetary Science Letters* **259**, 212–225. doi:10.1016/j.epsl.2007.04.043.

PÊCHER A., SEEBER L., GUILLOT S., JOUANNE F., KAUSAR A., LATIF M., MAJID A., MAHÉO G., MUGNIER J. L., ROLLAND Y., VAN DER BEEK P. & VAN MELLE J. 2008. Stress field evolution in the northwest Himalayan syntaxis, northern Pakistan. *Tectonics* **27**, TC6005.

REITER K., KUKOWSKI N. & RATSCHBACHER L. 2011. The interaction of two indenters in analogue experiments and implications for curved fold-and-thrust belts. *Earth and Planetary Science Letters* **302**, 132–146.

REPLUMAZ A. & TAPPONNIER P.2003. Reconstruction of the deformed collision zone between India and Asia by backward motion of lithospheric blocks. *Journal of Geophysical Research* **108**, doi:10.1029/2001jb000661

SEEBER L. & PÊCHER A. 1998. Strain partitioning along the Himalayan arc and the Nanga Parbat antiform. *Geology* **26**, 791–794.

SCHELLART W. P 2000. Shear test results for cohesion and friction coefficients for different granular materials: scaling implications for their usage in analogue modelling. *Tectonophysics* **324**, 1–16.

SCHELLART W. P. & LISTER G. S. 2005. The role of the East Asian active margin in widespread extensional and strike-slip deformation in East Asia. *Journal of the Geological Society* **162**, 959–972. doi:10.1144/0016-764904-112

SCHNEIDER D. A., EDWARDS M. A., KIDD W. S. F., ASIF KHAN M., SEEBER L. & ZEITLER P. K. 1999. Tectonics of Nanga Parbat, western Himalaya: Synkinematic plutonism within the doubly vergent shear zones of a crustal-scale pop-up structure. *Geology* **27**, 999–1002.

SCHREURS G., BUITER S. J. H., BOUTELIER D. *et al*. 2006. Analogue benchmarks of shortening and extension experiments. *Geological Society Special Publication* **253**, 1–27. doi:10.1144/GSL.SP.2006.253.01.01

SMIT J. H. W., BRUN J. P. & SOKOUTIS D. 2003. Deformation of brittle–ductile thrust wedges in experiments and nature. *Journal of Geophysical Research* **108**, B10. doi:10.1029/2002JB002190

ZHAO W., NELSON K. D. & PROJECT INDEPTH TEAM 1993. Deep seismic-reflection evidence continental underthrusting beneath southern Tibet. *Nature* **366**, 557–559.

Received 6 December 2011; accepted 29 May 2012